Ambient seismic noise imaging for tailings storage facilities monitoring: a benchmark between accelerometers and DAS

Lilas Vivin[1*], *Cristina* Vulpe[2], *Louise* McNab[3], *Andy* Fourie[2], *Johan* Boshoff[3], *Neil* Lester[3], *Caifang* Cai[1], *Thibaut* Allemand[1], *Jean* Lepine[1], *Thomas* Bardainne[1]

[1]*Sercel, Infrastructure Monitoring, 27 Avenue Carnot Massy, France*
[2]*The University of Western Australia, Department, 35 Stirling Highway, Crawley, Australia*
[3]*Gold Fields, Australia*
[*] *Corresponding author: Lilas.vivin@sercel.com*

ABSTRACT

Recent examples of tailings dam failure remind us how the monitoring of such sites is important. One major factor affecting the stability of tailings storage facilities (TSFs) is the presence and movement of water within the facility. Dam failures are often caused by seepage or the presence of weak layers within the tailings dam or the foundation soil. Thus, monitoring for the presence or movement of water within TSFs is becoming increasingly important, and solutions for permanent, non-intrusive and cost-effective monitoring of dams are a major challenge. One such solution is represented by geophysical imaging techniques such as ambient seismic noise interferometry. Through a research project, a nodal network system of accelerometer sensors was installed in a dense and random array on a TSF embankment wall at an Australian mine. Simultaneously, a fiber optic cable was deployed in a trench at the top of the TSF. Ambient seismic noise was recorded over a few weeks using the nodal network and with the fiber optic cable over several months using Distributed Acoustic Sensing (DAS) technology. Following data acquisition, benchmarking passive seismic imaging from the accelerometer network and the DAS system was conducted to evaluate the DAS capabilities for long-term TSF monitoring.

Keywords: ambient seismic noise; interferometry; surface waves; tailings storage facilities; monitoring; accelerometers, DAS.

1. Introduction

Tailings storage facilities (TSFs) are almost invariably already equipped with some form of monitoring instrumentation, but this instrumentation is not always appropriate, and the information obtained is sometimes irrelevant. The recent Jagersfontein dam failure in South Africa in September 2022 and the Williamson tailings dam failure in Tanzania in November 2022 confirm that an instrumented TSF is not necessarily, by definition, a safe TSF. Recent published literature has shown how some monitoring instrumentation recorded anomalies in TSF behaviour, such as accelerated changes in deformations of slopes, which were hypothesised to have been clear precursors to failure. All of these monitoring instrumentation data analyses were done post-failure. To the authors' knowledge there is no available literature on *a priori* detection of precursors to TSF failures.

One of the major factors affecting the structural health of a TSF is the change in the tailings' water content and level over the life of the facility. Geophysical imaging techniques, such as ambient seismic noise interferometry, represent a potential solution for permanent, non-intrusive monitoring which is able to track the water content changes through changes in shear wave velocity profiles and thus, help to image the structural health of the TSF. Ambient seismic noise interferometry is a passive seismic monitoring technique taking advantage of the low amplitude seismic waves generated during generic mine site activities.

The objective of this paper is to report, compare and validate ambient seismic noise interferometry results from a short monitoring campaign of a TSF instrumented with fiber optic cables (i.e., distributed acoustic sensors) and a temporary array of 469 self-powered seismic sensors.

2. Instrumented TSF area

Figure 1. Western Australia gold mine – TSFs area of interest (green square).

The chosen site location to install the fiber optics cables and the temporary array of self-powered seismic sensors is located at a gold mine in Western Australia. The area of interest that was instrumented corresponds to the dam slope along one of the 'cells' of the TSF (Fig. 1). In September 2022, a nodal network of 469 seismic sensors was deployed on the TSF embankment wall. The WiNG^{NT} sensors used for this acquisition are self-powered nodes containing QuietSeis^{TM} MEMS accelerometers.

Three lines of seismic sensors, referred as 'nodes' in this paper, were positioned at three different levels along the embankment wall:

- Line 1 (L1) at the top of the TSF: composed of 134 nodes aligned along 136m with 1m spacing.
- Line 2 (L2) at a mid-level from the top: composed of 143 nodes aligned along 150m with 1m spacing.
- Line 3 (L3) at a third lower layer: composed of 76 nodes aligned along 150m with 2m spacing.

Additionally, 116 nodes were installed in a random pattern on the TSF beach close to the embankment wall and on the slope of the TSF, while maintaining a 10m spacing between nodes on average.

GPS positions of the nodes were precisely surveyed by means of real-time kinematic GPS receivers. The nodes' locations on the TSF are schematically represented by yellow dots in Fig. 2.

All nodes were buried in very shallow trenches and partially covered with tailings. Afterwards, the nodes were switched on and allowed to record ambient seismic noise on the TSFs area for one month with 1000 Hz sampling rate.

At the same time, a fiber optic cable was buried in a shallow trench located on the TSF beach, close to the embankment wall. The fibre optic is schematically shown as a purple line in Fig. 2. A total of 530m of straight fiber optic cable was deployed in the trench and then covered with the tailings material, which allows for a good coupling of the fiber.

The first section of the fiber optic cable was deployed alongside the L1 line of nodes (schematically shown as a green line in Fig 2) to enable a comparison between fiber optics and nodal data results in a similar context (Fig. 3).

A Distributed Acoustic Sensing (DAS) interrogator was located inside an air-conditioned container to record the seismic ambient noise on the TSFs continuously. DAS acquisition parameters are shown in "Table 1".

Table 1. DAS acquisition parameters

Parameters	**Values**
Pulse rate	20 kHz
Spatial sampling	5m
Gauge length	10m

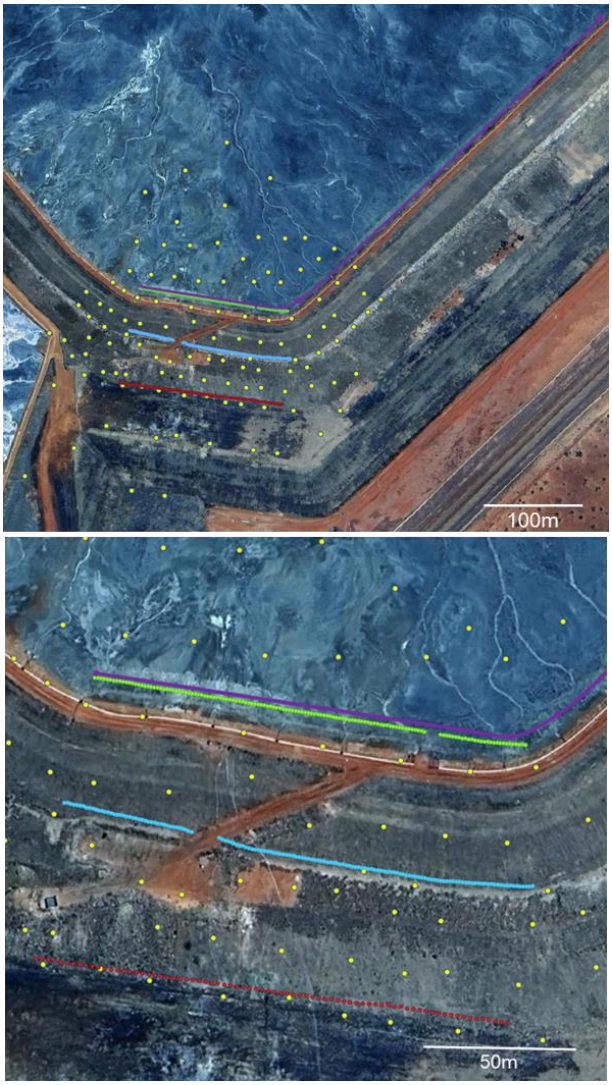

Figure 2. Acquisition layout – Top: global scale, Down: zoom on the dam slope. Yellow points - random nodes; red points - nodes on L3; blue points - nodes on L2; green points - nodes on L1; purple line - fiber optic path.

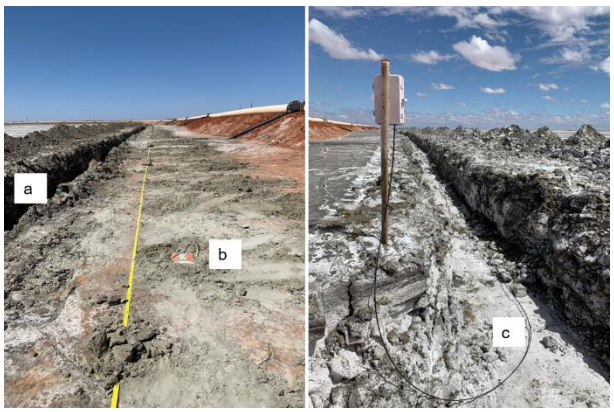

Figure 3. Photo of the equipment installed on the TSFs. a) Trench for the fiber optic cable – b) Nodal accelerometer WiNG (L1) – c) Straight fiber optic cable

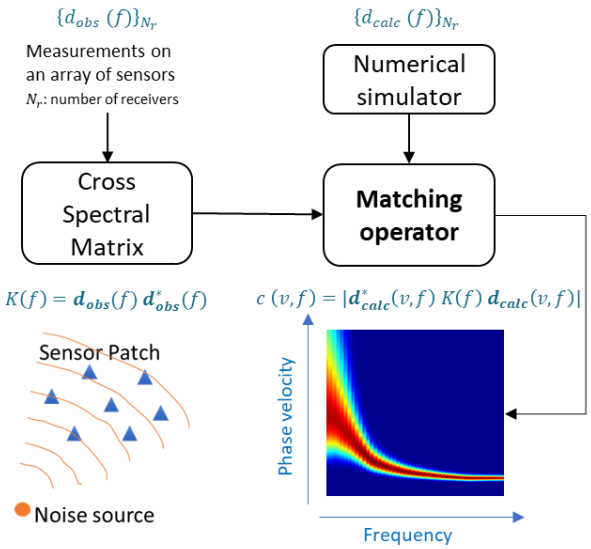

Figure 4. Single patch representation and algorithm of generic MFP with Bartlett processor

3. Methodology

3.1. Interferometry

Ambient seismic noise can be used for underground imaging (Campillo & Paul, 2003, Campillo *et al.*, 2011). The cross-correlation of a signal recorded by a pair of receivers A and B can create a virtual source-receiver pair respectively from A to B. Surface waves are particularly suitable for interferometry. An important requirement that controls the efficiency of interferometry is the alignment between the source and the receiver array. Interferometry is based on ambient seismic noise recordings (Dou *et al.*, 2017, Chang et al., 2016), considering that the random distribution of noise sources provides both constructive alignments and destructive misalignments.

Virtual gathers are built from the cross-correlations over the recording time period.

3.2. Matched field processing

The next post-processing step is the computation of the dispersion diagrams. This step involves an adaptation of Matched Field Processing (MFP) (Jensen *et al.* 2011, Chmiel *et al.*, 2016). Considering the known positions of a patch array of sensors, MFP is used to reconstruct the highly sensitive phase, known as the Bartlett operator, namely B, and the group velocity panels (Fig. 4).

The principle of MFP is to match wave propagation measurements for an array of sensors with numerical simulations. Using a numerical simulator, the propagation medium velocity is scanned to find the best match with the wave field recorded by a given patch of sensors. This process is repeated for each angular frequency ω, and a dispersion curve (i.e., surface-waves phase velocity, v, as a function of the angular frequency ω) is built.

More specifically, given a patch of receivers r_j, where $1 \leq j \leq N$, and the positions of sources s_i,where $1 \leq i \leq M \ll N$, $d_{ij}(\omega)$ represents the cross-correlation of data recorded at s_i and r_j, in the frequency domain. For a given trial velocity v, $p_{ij}(\omega, v) = e^{\frac{2i\pi\omega l_{ij}}{v}}$ represents the trial phase, with l_{ij} the distance between s_i and r_j. The Bartlett operator between two receivers, j_1 and j_2, is given by:

$$B(\omega, v) = \left| \sum_{i=1\ldots M} \sum_{j_1, j_2 = 1\ldots N} p_{ij_1}(\omega, v) d_{ij_1}(\omega) \bar{d}_{ij_2}(\omega) \bar{p}_{ij}(\omega, v) \right|$$

If $d_i(\omega)$ is the vector of all the $d_{ij}(\omega)$ and $p_i(\omega, v)$ is the vector of all the $p_{ij}(\omega, v)$, then using the cross spectral matrix $K_i(\omega) = d_i(\omega) d_i^H(\omega)$ with H denoting the transpose conjugate, B(ω, v) becomes:

$$B(\omega, v) = \left| \sum_{i=1\ldots M} p_i^H(\omega, v) K_i(\omega) p_i(\omega, v) \right|$$

The Rayleigh phase velocity is then taken at the maximum, namely:

$$v(\omega) = \arg\max_v B(\omega, v)$$

An equivalent computation can be performed with the envelope of the signal to obtain the group velocity information.

The dispersion curves $v(\omega)$ obtained for each patch of sensors are then input in a tomography analysis in order to correct for the averaging effect of the patches. Thanks to a great variety in both the size and position of the patches (and the associated overlap), this tomography

results in a resolution that is almost half of the typical distance between sensors. The multichannel analysis of surface waves (MASW) method, by comparison, is generally limited to twice the distance between sensors.

3.3. Surface waves inversion

Following MFP processing, a depth-inversion is performed on the X-Y-frequency phase velocity volume output from the tomography. The result is a three-dimensional (3D) X-Y-Z volume of shear-waves velocity profiles.

4. Results

4.1. Nodal & DAS processing

The surface waves imaging method described above was first applied to the data acquired from the random array of nodes to obtain a global 3D image of the tailings dam. Cross-correlations were calculated on 9 consecutive days of ambient seismic noise recording and stacked to get virtual gathers (Fig. 5.a). Dispersion diagrams were then computed by means of MFP (Fig. 1.b). Tomography and multi-waves inversions were finally applied to obtain the final image, a 3D S-wave velocity model of the tailings dam area.

The same processing sequence was applied to the data from the line of nodes L1 located on the TSF beach alongside the fiber optic cable, which permits a direct comparison between the nodal and DAS results. Virtual gathers and dispersion curves from L1 are illustrated in Fig5.c. and Fig5.d., respectively.

The data acquired by means of fiber optic cable were processed as two separated linear sections: a first section of approximately 135m located alongside the dense line of nodes L1, and a second section of 380m. The current study presents the results of the 135m long section parallel to the line of nodes L1.

Cross-correlations were calculated on 8 consecutive days of ambient seismic noise recording and stacked to get virtual gathers (Fig. 5.e). Dispersion curves were then computed using MFP (Fig. 5.f). Finally, a 2D S-wave velocity model along the fiber was obtained using tomography and multi-wave inversion, as described in the Methodology section.

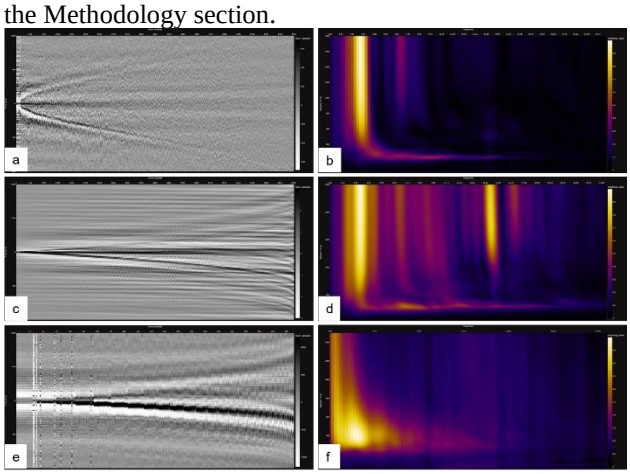

Figure 5. a) Virtual gathers from the 3D nodal network – b) Dispersion curve example from the 3D nodal network – c) Virtual gathers from the line of nodes L1 – d) Dispersion curve example from the line of nodes L1 e) Virtual gathers from DAS data – f) Dispersion curve example from DAS data.

4.2. 2D & 3D S-wave velocity models

4.2.1. 3D S-wave velocity model from the 3D nodal network

Shear wave (S-wave) velocity profiles along the X and Y directions, referred to as X slice and Y slice, with their position schematically illustrated in Fig 6, are shown in Fig 7 and Fig 8 for the 3D nodal network located on the slope of the TSF at three depth intervals, namely 25m, 35m and 45m respectively. The 2D nodal network is represented by the nodes located on the L1, L2 and L3 lines.

S-wave velocity profiles along the Y slice are shown in Fig.9 for the 3D nodal network, L1 nodes and the fiber optic cable, respectively.

We observe structural features on velocity model that are consistent with expected structure of the dam itself. Note that resolution is coarser using DAS. This is due to the intrinsic spatial filtering induced by the use of a gauge length of 10 meters, that naturally loses the high frequency content of the surface waves but also decreases the lateral resolution.

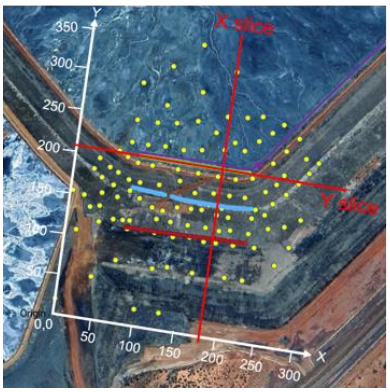

Figure 6. X & Y slices location map

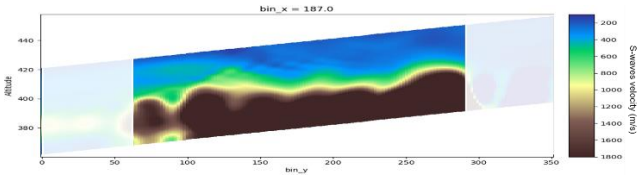

Figure 7. S-wave velocity X slice from the 3D nodal network.

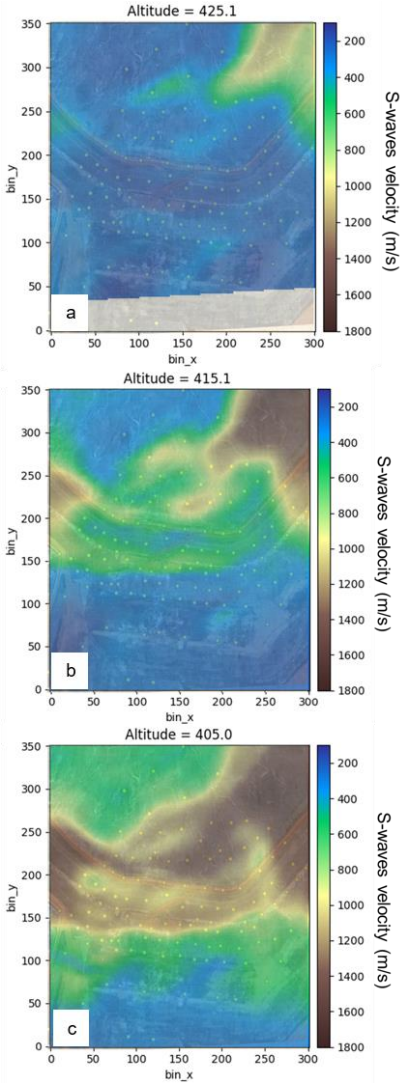

Figure 8. S-wave velocity depth slices from the 3D nodal network extracted at different elevation levels. a) 25m deep – b) 35m deep – c) 45m deep.

4.2.2. Benchmark between nodal and DAS results

S-wave velocity models from 3D and linear nodal acquisition show very close S-wave velocity variations with depth along the shown sections. A decrease in the velocity can be observed from around 400m/s at the top of the section to 200m/s at approximately 20m depth. Afterwards, the S-wave velocity increases and reaches almost 400m/s at 30m depth, 700m/s at 40m depth and 1800m/s at 50m depth. The S-wave velocity profile obtained from the DAS data shows very similar variations but with lower velocities.

Data from the L1 nodal acquisition shows a better resolution due to the 1m spatial sampling between nodes compared to the 5m spatial sampling for DAS. The 10m gauge length, which represents the distance separating two positions on the fiber optic cable, is also acting as a natural filter that limits the high frequencies recorded on DAS data. Thus, data acquired by the nodes includes high frequencies, leading to a better resolution.

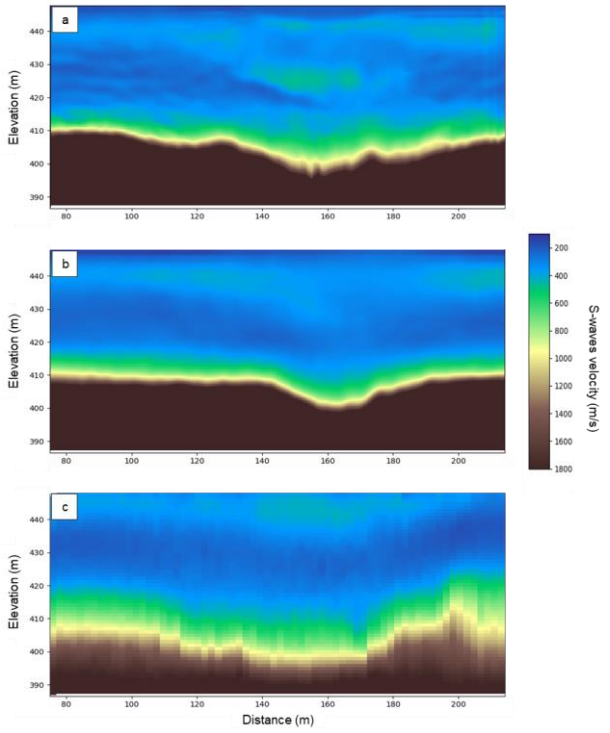

Figure 9. S-wave velocity Y slice. a) from the 3D nodal network – b) from the line of nodes L1 – c) from the DAS section.

S-wave velocity models from nodal and DAS data may be compared with the shear-wave velocity profile from seismic piezocone testing (sCPT-u). The current monitoring instrumentation campaign was carried out in an area of the TSF for which a number of sCPTs were also conducted independently by an external contractor, as shown in Fig 10.a. The S-wave velocity profiles obtained by means of nodal and fiber optics instrumentation are compared to the sCPT data from location G1.

The sCPT-u at location G1 reports a point-wise S-wave profile from the TSF beach surface up to a 30m depth. This profile shows first a decrease of the S-wave velocity from 450m/s at the top to 200m/s at 17m depth, followed by an increase up to 300m/s at 32m depth. The evolution of the S-wave velocity profile is very close to that obtained from the nodal data, expect the increase of S-wave velocity in the shallowest 5 meters, that is not measurable with ambient noise. However, sCPT-u data acquisition represents a single point on the TSF at a particular point in time. Additionally, in order to obtain additional sCPT profiles, a new campaign of field testing is required, which includes access to external personnel at the mine site. The sCPT testing can only be carried out at specific times while tailings are not discharged into the impoundment. On the contrary, nodal or DAS instrumentation allows for 2D or 3D S-wave velocity continuous monitoring, which, once installed on the TSF, can occur during tailings deposition periods.

4.3. Discussion

One aspect that should be considered in the ambient seismic noise interferometry is the impact of the noise source location in the case of a linear acquisition if the

noise is not isotropic. In the study, seismic sensors are vertical and record Rayleigh waves only, while DAS is sensitive to waves collinear to the fiber cable and can therefore record both Rayleigh and Love waves, depending on the position of the noise source. This aspect may also explain the velocity differences that can be observed between DAS and nodal results. An ambient seismic noise analysis, preliminary to the acquisition layout definition, could help position the DAS fiber.

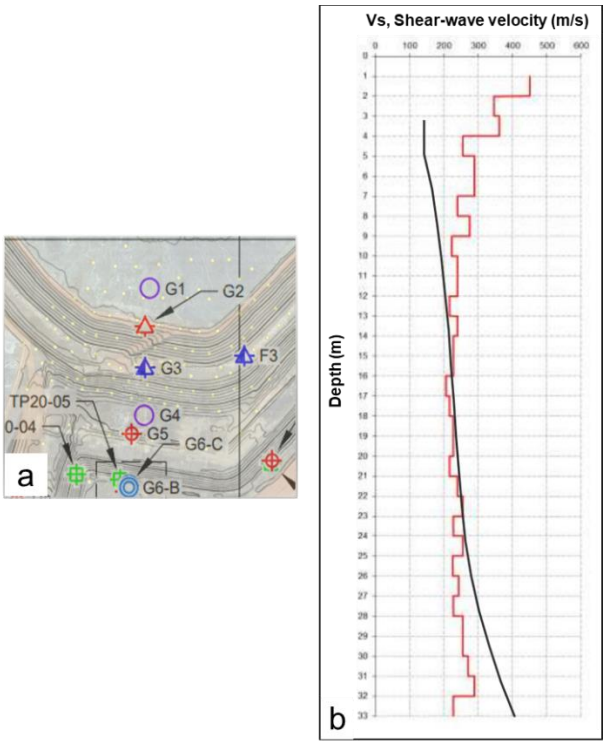

Figure 10. a) Field investigation map on the TSFs embankment wall – b) Shear-wave velocity profile for SCPT-u at G1 location in red and extraction of S-wave velocity profile from model obtained using nodal acquisition in black.

5. Conclusion

This study reports ambient seismic noise interferometry results from a short period monitoring campaign of a TSF located in Western Australia instrumented with fiber optic cables (i.e., distributed acoustic sensors) and a temporary array of 469 self-powered seismic sensors. Three lines of seismic sensors, referred to as 'nodes' in this paper, were positioned at three different levels along the embankment wall. A fiber optic cable was buried in a shallow trench located on the TSF beach, close to the embankment wall and alongside the topmost line of nodes. This arrangement allowed for a comparison and validation of the DAS data against the seismic sensors.

The S-wave velocity profiles obtained from the nodes and DAS data show very similar variations, with DAS reporting slightly lower velocities.

The S-wave velocity profiles generated by the nodes show a better resolution due to the 1m spatial sampling between nodes compared to the 5m spatial sampling for DAS.

The S-wave velocity profiles from the nodes and DAS were also validated against a sCPT profile, showing good agreement between the three instrumentation options.

DAS data have been recorded for six consecutive months on the area of interest of the TSF. The results presented in this paper only come from the processing of eight consecutive days of data acquired at the beginning of the installation in September 2022.

With a perspective towards long-term monitoring, the processing of a week of DAS data every month will be initiated soon. This will allow for the long-term analysis of the health of the TSF by giving information on temporal changes in shear wave velocities within the tailings impoundment and, by extension, information on the changes in water content. Measurements of water fall and temperature should be taken into account to better distinguish "expected" variation of time from anomaly revealing the genesis of a disorder

Acknowledgements

The authors would like to gratefully acknowledge funding awarded from the Amira P1217 Evaluation of Tailings Storage Facilities monitoring technologies Project, funded through Amira Global by Gold Fields, Agincourt Resources, Boliden, Anglo American, Lundin Mining, Rio Tinto, Independence Group, CMOC, BHP, LKAB, ArcelorMittal, 3vGeomatics, Ground Probe, Institute of Mine Seismology, CGG Services UK, Sercel, Canary Systems and Loupe Geophysics.

References

Campillo, M. & Paul, A., 2003. "Long-range correlations in the diffuse seismic coda", In *Science*, 299(5606), 547. 18, 87.

Campillo, M., Roux P. and Shapiro, N. M., 2011. "Correlation of seismic ambient noise to image and monitor the solid Earth", In *Encyclopaedia of Solid Earth Geophysics*, Springer Science + Business Media B.V. 22, 54, 128. https://doi.org/10.1007/978-90-481-8702-7

Chang J. P., de Ridder S.A. and Biondi B. L., 2016. "High-frequency Rayleigh-wave tomography using traffic noise from Long Beach, California", In Geophysics, 81: B43-B53.

Chmiel M., Roux P. and Bardainne T., 2016. **"**Extraction of phase and group velocities from ambient surface noise in a patch-array configuration", In *Geophysics*, 81, 6, 231-240.

Dou, S., Lindsey, N., and Wagner, A.M., 2017. "Distributed Acoustic Sensing for Seismic Monitoring of the Near Surface: A Traffic-Noise Interferometry Case Study", In Nature, Sci Rep 7, 11620.

Jensen, F. B., Kuperman, W. A., Porter, M. B., and Schmidt, H., 2011. "Computational Ocean Acoustics", 2nd ed. New York: Springer-Verlag. *https://doi.org/10.1007/978-1-4419-8678-8*